Sensors and Actuators B 185 (2013) 445–455

Contents lists available at SciVerse ScienceDirect

Sensors and Actuators B: Chemical

journal homepage: www.elsevier.com/locate/snb

Low-temperature and highly selective NO-sensing performance of WO_3 nanoplates decorated with silver nanoparticles

Deliang Chen[a,*], Li Yin[a], Lianfang Ge[a], Bingbing Fan[a], Rui Zhang[a,b], Jing Sun[c], Guosheng Shao[d,e]

[a] School of Materials Science and Engineering, Zhengzhou University, 100 Science Road, Zhengzhou 450001, PR China
[b] Laboratory of Aeronautical Composites, Zhengzhou Institute of Aeronautical Industry Management, University Centre, Zhengdong New District, Zhengzhou 450046, PR China
[c] The State Key Laboratory of High Performance Ceramics and Superfine Microstructure, Shanghai Institute of Ceramics, Chinese Academy of Sciences, 1295 Dingxi Road, Shanghai 200050, PR China
[d] UK-China Centre for Multi-functional Nanomaterials, Zhengzhou University, Zhengzhou 450001, PR China
[e] Institute for Renewable Energy and Environmental Technology, University of Bolton, Bolton BL3 5AB, UK

ARTICLE INFO

Article history:
Received 29 January 2013
Received in revised form 20 April 2013
Accepted 1 May 2013
Available online 9 May 2013

Keywords:
Ag/WO_3 nanocomposite
Nitric oxide (NO)
Chemical sensor
Low-temperature sensing
Selectivity

ABSTRACT

For improving the low-temperature response and selectivity of WO_3-based sensors, Ag nanoparticles (AgNPs) have been used to modify the WO_3 nanoplates. Ag@plate-WO_3 nanocomposites with various amounts of AgNPs were synthesized by growing AgNPs on WO_3 nanoplates. XRD, SEM, TEM and XPS spectrum were used to characterize the Ag@plate-WO_3 samples. The gas-sensing properties were evaluated at r.t. −250 °C using NO gases with various concentrations (0.5–50 ppm). AgNPs enhance the low-temperature response and selectivity of the Ag@plate-WO_3 sensors for NO detection, and the amounts of AgNPs influence the NO-sensing performance of the Ag@plate-WO_3 sensors. The sample with 0.5% AgNPs shows the best performance. Its optimum operating temperature is around 170 °C, but it shows response even at room temperature. The Ag@plate-WO_3 sensors have a high selective response to NO gas, among various gases (i.e., H_2 and CO) and organic vapors (i.e., alcohol, acetone, methanol and benzene). The morphologies of WO_3 nanocrystals also influence the NO-sensing properties of the Ag@WO_3 sensors, and the plate-like WO_3 samples are better than the particle-like WO_3 samples in improving NO-sensing performance. The NO-sensing enhancement should result from the synergistic effects of AgNPs and the loose house-of-card structure of plate-like WO_3 aggregates.

1. Introduction

Chemical sensors based on semiconductive metal oxide nanostructures (SMONs) have wide applications in various industries and environment control [1–5]. Fabrication and performance evaluation of the SMON sensors have attracted increasing attention in recent decades [6–12]. Not the sizes but the exposed facets of the SMONs have effects on their gas-sensing performance [13]. Various synthetic methods have been developed to achieve SMONs with various morphologies and dimensions for sensing applications [7,14,15]. The SMON sensors can be sensitive to various gases (e.g., H_2 [3], NH_3 [16], CO [17], and NO_x [18]) and organic vapors (e.g., ethanol [14], acetone [19], and benzene [20]). Although wide investigations on the SMON sensors have been done, how to enhance the sensitivity, how to improve the selectivity, and how to reduce the working temperature are still challenges in development of high-performance chemical sensors [21].

Nitric oxides (NO_x: NO and NO_2) are common toxic gases generated by the burning of coal, seriously harmful to environment and human being's health [22]. To develop NO_x-sensing sensors with high performance for environmental monitoring and control is a significant research topic [15,23–25]. The SMON sensors, including In_2O_3 nanoparticles (NPs) [26], porous SnO_2 powders [27], TiO_2/ZnO double films [28], SnO_2/In_2O_3 nanocomposites [29], ZnO hollow hemisphere and urchin-like structures [30], and MoO_3 [31], have been reported for NO_x detection. However, to meet the requirements of high sensitivity, low operation temperature and good selectivity at the same time is still a great challenge for NO_x sensors [15,23,25–27,30].

Modifying SMONs with noble metal NPs [31–38] and other functional species [21,27,39] is an efficient way to improve the their gas-sensing performance [40]. Zhang et al. found that Au NPs can enhance the sensitivity and shorten the response time of ZnO nanoplate sensors for ethanol vapors [33]. Liu et al. found that the addition of Au NPs into ZnO flowers led to improved

* Corresponding author. Tel.: +86 371 67781046; fax: +86 371 67781593.
E-mail addresses: dlchen@zzu.edu.cn, dlchennano@hotmail.com (D. Chen).

0925-4005/$ – see front matter © 2013 Elsevier B.V. All rights reserved.
http://dx.doi.org/10.1016/j.snb.2013.05.006

sensor response, selectivity and short response and recovery times to acetone vapors via the formation of Au/ZnO hybrids and surface coarsening of ZnO flowers [41]. Lee et al. reported the room-temperature sensing of Au NP-functionalized In_2O_3 nanowire field-effect transistor (NW-FET) for low-concentration CO gases, and found that the presence of Au NPs on the surface of In_2O_3 nanowire serves to enhance the CO oxidation due to a higher oxygen ion-chemisorption on the conductive Au NP surfaces [42]. Xue et al. reported Pd–ZnO nanoflower sensors with high sensitivity, fast response, high selectivity and low work temperature, and attributed the enhanced performance to Schottky contact at the Pd/ZnO interface and catalytic activity of Pd NPs [43]. Yuasa et al. reported H_2-sensing Pd/SnO_2 sensors which show that Pd has a large electrical sensitization effect (e.g., enhancement in sensitivity and reduction in operating temperature) by efficiently catalytic combustion of H_2 on Pd [44]. Zhou et al. found that the modification of Au, Pd, and Pt NPs to homogeneous In_2O_3 NPs thin film sensors enhanced the sensitivity to H_2S, H_2 and CO, respectively [45]. Lee et al. reported the effect of Ag decoration on the gas sensing characteristics of SnO_2 nanowire (NW) networks, and found that isolated Ag nano-islands enhance the C_2H_5OH response, whereas continuous Ag decoration layers reduce the response to C_2H_5OH, compared to pristine SnO_2 NWs [46]. Chen et al. reported a selective, room-temperature NH_3 gas sensing platform with enhanced sensitivity, superfast response and recovery, and good stability, using Ag nanocrystal-functionalized multiwalled carbon nanotubes [47].

Tungsten oxide (WO_3), an *n*-type semiconductor with a bandgap of 2.5–2.8 eV, has important applications in various fields [7,48–53]. WO_3-based nanomaterials with various morphologies have been widely investigated for chemical gas sensors [20,54–62], to detect NH_3 [16], H_2 [63], ethanol [64–66], modified with Au NPs and Pt NPs. Very recently, we developed a topochemical approach to synthesize two-dimensional WO_3 nanoplates with a single-crystal structure and high specific surface areas [67], and the as-obtained WO_3 nanoplates showed highly sensitive to the vapors of alcohols [68] and acetone [19].

WO_3-based materials are also useful in NO_x detection [69–72]. Square-like WO_3 nanosheets synthesized by hydrothermal treatment [73], atmospheric plasma-sprayed WO_3 coating [74], ultrafine WO_3 NPs by a nanocasting route [75], WO_3 hollow microspheres [76], lamellar-structured WO_3 particles by an acidification method [77], porous WO_3 by anodizing sputtered tungsten thin film [78], mesoporous WO_3 by a silica template method [79] and monoclinic WO_3 film by aerosol assisted chemical vapor deposition [80] are reported for NO_2-sensing application. The addition of metal NPs and carbon nanotubes can improve the sensing performance of WO_3 sensors for NO_2 detection [80,81]. Comparatively, the WO_3 sensors for NO-sensing applications are seldom reported [18,61,82]. To the best of our knowledge, WO_3 nanoplates decorated with Ag NPs for the NO-sensing application have not been reported yet.

In this paper, we introduce a novel Ag@plate-WO_3 nanocomposite for NO-sensing application by photo-induced growth of Ag NPs on single-crystalline WO_3 nanoplates, which are synthesized via a topochemical intercalation approach [67,84]. The effects of Ag NPs on the NO-sensing performance (i.e., sensitivity, selectivity and response times) of the Ag@plate-WO_3 sensors are systematically investigated. In addition, the influences of WO_3 morphologies (e.g., nanoplates and NPs), operation temperatures, the amounts of Ag NPs on the NO-sensing property are also investigated. The results indicate that the Ag@plate-WO_3 sensors have highly selective response upon exposure to NO gases (0.5–100 ppm) at a large operation temperature window (25–200 °C). The related mechanism for the enhanced NO-sensing performance of the Ag/plate-WO_3 sensors is carefully discussed.

2. Experimental

2.1. Synthesis of Ag@plate-WO_3 nanocomposites

WO_3 nanoplates were synthesized on the basis of intercalation chemistry and topochemical approach according to the previous reports [67,84]. Tungstic acid (H_2WO_4) reacted with n-octylamine to form tungstate-based inorganic–organic hybrid belts (THBs) using heptane as the solvent. The molar ratio of n-octylamine to H_2WO_4 is 8:1, and the volume ratio of heptane to n-octylamine is about 8:1. The as-obtained THBs were then treated with a HNO_3 aqueous solution (~6 mol/L) to remove organic species, and two-dimensional H_2WO_4 nanoplates were obtained. The H_2WO_4 nanoplates obtained were finally calcined at 400 °C for 2 h in air to synthesize WO_3 nanoplates.

Ag@plate-WO_3 nanocomposites were synthesized by a photo-induced reducing method using the above WO_3 nanoplates as the substrate. Typically, polyvinylpyrrolidone (PVP K30) and WO_3 nanoplates were dispersed in an ethanol/water (7:3 in volume) mixture under magnetic stirring, and a $AgNO_3$ aqueous solution was then added into the above PVP–WO_3 suspension. The as-obtained Ag^+–PVP–WO_3 suspension was finally irradiated by a Xenon lamp (350 W) for ~1 h. In the precursors, the molar ratio of the repeat unit of PVP to Ag is 5:1, and the mass ratios of Ag to WO_3 were 0.25%, 0.5%, 1% and 2%, respectively. The solids were collected by filtration, washed with H_2O/ethanol mixtures thoroughly, and then dried at 80 °C in a reduced pressure. The as-obtained samples were marked as *x*%Ag@plate-WO_3, and the *x* values were 0, 0.25, 0.5, 1 and 2, respectively.

For the purposes of comparative study, WO_3 nanoparticles were synthesized by calcining H_2WO_4 nanoparticles at 500 °C for 1 h. The *x*%Ag@particle-WO_3 composites with WO_3 nanoparticles were synthesized using the similar method.

2.2. Characterization of phases and microstructures

The phases of the Ag@WO_3 samples were determined by XRD patterns (X'Pert Pro X-ray diffractometer equipped with Cu Kα radiation). The TEM, HRTEM images and SAED patterns were recorded on a Tecnai-G 20 transmission electron microscope with an acceleration voltage of 200 kV. SEM images were obtained using a JEOL-6700F scanning electron microscope.

2.3. Fabrication of WO_3 and Ag@WO_3 sensors

The WO_3 and Ag@WO_3 sensors were fabricated according to the previous reports [68]. The Ag@plate-WO_3 nanocomposites were mixed with a small amount of de-ionized H_2O/ethanol mixture to form a paste in a glass dish. The Ag@plate-WO_3 paste was then brush-coated onto the surface of an Al_2O_3 microtube with four Pt electrodes. After the Ag@plate-WO_3 coating was air-dried, the coating process was repeated until a continuous coating was formed. The Ag@plate-WO_3-coated Al_2O_3 microtube was then fixed to a special pedestal with 6 poles by welding the four Pt electrodes to 4 poles of the pedestal, respectively. A heating coil (Ni–Cr) was then inserted through the Al_2O_3 microtube and its two ends were welded to the other two poles of the pedestal. A schematic diagram of the Ag@plate-WO_3 sensor was shown in Scheme 1(a). The other sensors with WO_3 nanoplates, WO_3 nanoparticles, and Ag@particle-WO_3 nanocomposites were fabricated used the similar process.

2.4. Measurement of the gas-sensing performance of Ag@WO_3 sensors

The gas-sensing test was conducted using a commercial computer-controlled WS-30A system (Zhengzhou Winsen

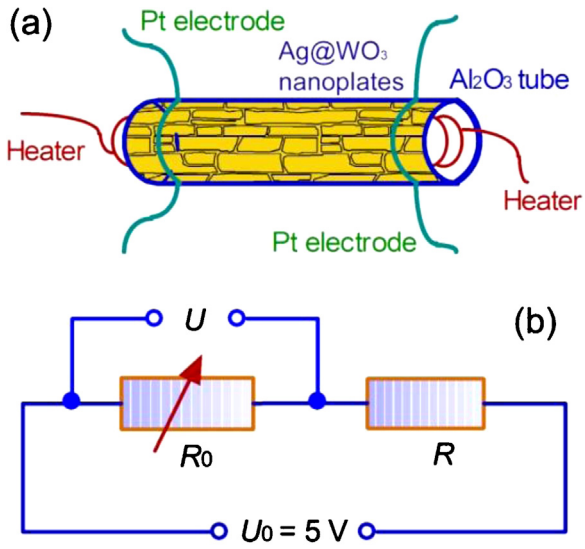

Scheme 1. (a) A schematic diagram of the Ag@plate-WO_3 sensor. (b) An equivalent circuit of the gas-sensing testing system used.

Electronics Technology Co., Ltd., Zhengzhou, China) under a static testing condition [19,68]. The sensors, integrated in a large circuit board with 32 inlet-sites, were encased in a transparent glass chamber with a volume of ~16.7 L. The test system was placed in a ventilating cabinet with a large draught capacity. NO was used as the target gas to evaluate the gas-sensing performance of the Ag@WO_3 sensors. To investigate the selectivity of the Ag@WO_3 sensors, some organic vapors (e.g., methanol, ethanol, isopropanol, methanol, acetone and benzene), CO, H_2, SO_2 and NO_2 were also used as the target substrates. The target gases were sampled using syringe-like samplers with a volume range of 1–10 μL. Their concentrations (0.5–100 ppm) were calculated according to the densities of liquid organic substrates and the volume of the chamber [19]. The operation temperatures varied from room temperature to 250 °C. The relative humidity (RH) of the environment was 16–50%.

An equivalent circuit of the gas-sensing test system is given in Scheme 1(b). The Ag@WO_3 sensor (R) is connected in series with the load resistor (R_0) with a known resistance, and a source voltage (U_0) of 5 V is loaded on the circuit. The system measures the voltages (U) loaded on the resistor R_0, and the resistances (R) of the WO_3 sensors can therefore be calculated according to Eq. (1) [68].

$$R = \frac{U_0 - U}{U} \times R_0 \quad (1)$$

For reducing gases (or vapors) and n-type semiconductor sensors, the sensitivity (S_r) is defined as Eq. (2); whereas for oxidizing gases and n-type semiconductor sensors, the sensitivity (S_r) is defined as Eq. (3). Here, R_a and R_g are the resistances of the WO_3-based sensors in air and in target gases, respectively.

$$S_r = \frac{R_a}{R_g} \quad (2)$$

$$S_r = \frac{R_g}{R_a} \quad (3)$$

The response time (τ_{res}) is defined as a duration in which the variation amplitude of the voltage of the load resistor is not larger than 5%, starting from the time point of gas-on. Similarly, the recovery time (τ_{rec}) is defined as a duration in which the variation amplitude of the voltage of the load resistor is not larger than 5%, starting from the time point of gas-off [68].

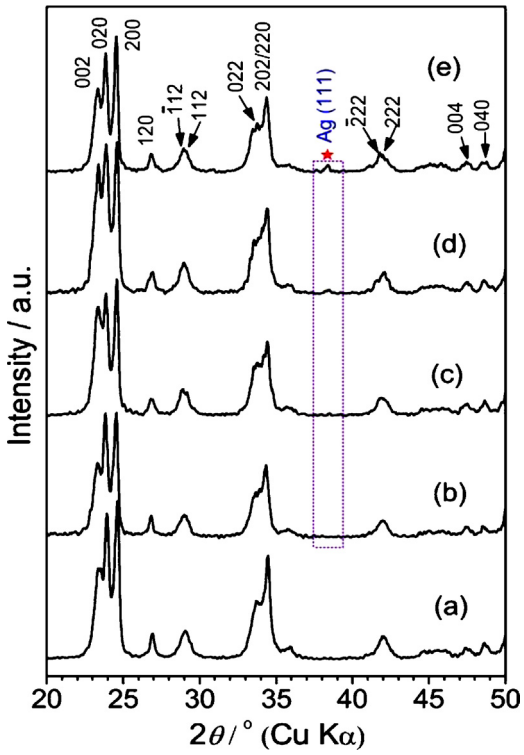

Fig. 1. XRD patterns of the Ag@plate-WO_3 nanocomposites with various amounts of Ag NPs: (a) pure WO_3 nanoplates, (b) WO_3 nanoplates with 0.25 wt.% Ag NPs, (c) WO_3 nanoplates with 0.5 wt.% Ag NPs, (d) WO_3 nanoplates with 1.0 wt.% Ag NPs, and (e) WO_3 nanoplates with 2.0 wt.% Ag NPs.

3. Results and discussion

3.1. Synthesis and characterization of Ag@plate-WO_3 nanocomposites

Single-crystalline WO_3 nanoplates were formed by an intercalation–topochemical approach, making good use of the inheritable two-dimensional [WO_6] layers in the precursors of tungstic acid [66,83]. A typical XRD pattern of the WO_3 nanoplates obtained was shown in Fig. 1a. It can be indexed to a triclinic WO_3 phase according to the JCPDS card No. 32-1395 [68]. The as-obtained WO_3 nanoplates are of a high specific surface area and good redispersibility [67].

The formation of Ag NPs on the surface of WO_3 nanoplates is achieved via a photo-induced reduction reaction shown as Eq. (4):

$$Ag^+ - PVP@plate\text{-}WO_3 \xrightarrow{UV-vis} Ag^0@plate\text{-}WO_3 \quad (4)$$

Fig. 1(b)–(e) shows the XRD patterns of the Ag@plate-WO_3 nanocomposites with various amounts of Ag NPs (0.25–2.0%). One can find that the peaks belonging to WO_3 phase are not changes, whereas a new peak located at 38.1°, belonging to the (1 1 1) deflection of face-centered cubic structured Ag (JCPDS card No. 04-0783), becomes stronger and stronger as the amount of Ag increases. The XRD results confirm the formation of metal Ag phase in the Ag@plate-WO_3 samples. The increasing intensity of the Ag (1 1 1) peak (marked by a star) indicates that the more the amount of Ag^+ in the precursor, the more the amount of the metal Ag in the Ag@plate-WO_3 nanocomposite.

SEM and TEM observations were used to characterize the microstructures of the as-obtained Ag@plate-WO_3 nanocomposites. Fig. 2 shows the typical results of sample 0.5%Ag@plate-WO_3. Fig. 2(a) shows a SEM image. The small particles marked with

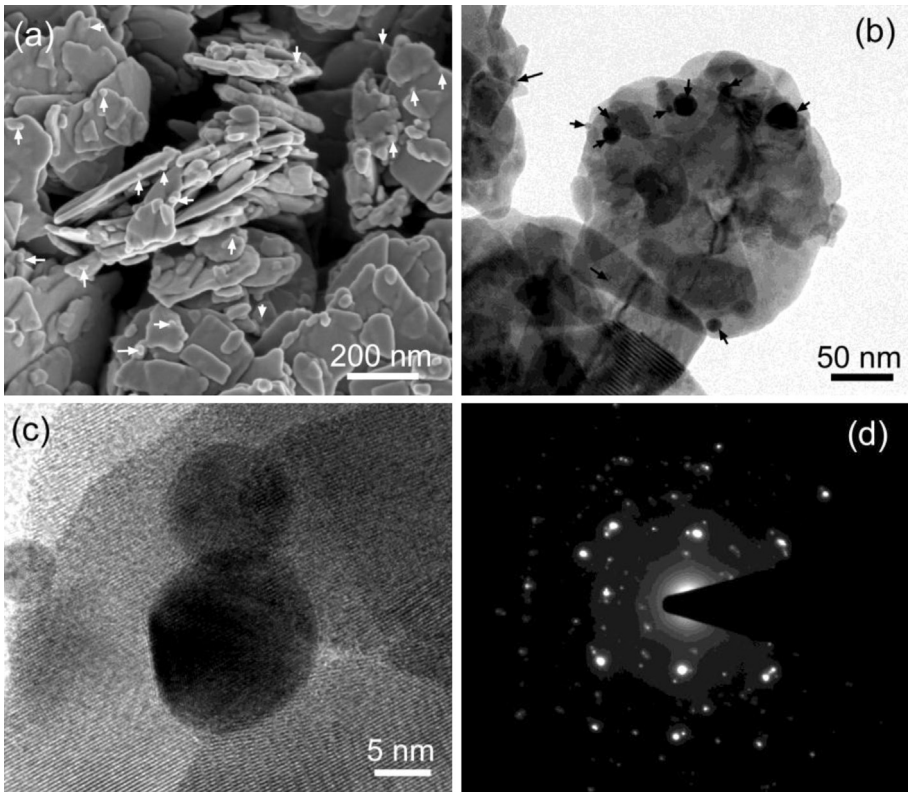

Fig. 2. SEM and TEM observations of the 0.5%Ag@plate-WO_3 nanocomposite: (a) SEM image, (b) low-magnification TEM image, (c) high-resolution TEM (HR-TEM) image, and (d) selected area electron diffraction (SAED) pattern.

arrows should be Ag NPs, which are attached on the surfaces of WO_3 nanoplates. The TEM image in Fig. 2(b) shows that the Ag NPs with small sizes are anchored on the surfaces of WO_3 nanoplates, similar to the SEM observation in Fig. 2(a). Fig. 2(c) shows an HRTEM image. One can find that the sizes of Ag NPs are 5–15 nm. The corresponding SAED pattern shown in Fig. 2(d) has two sets of diffraction spots: the bright spots belonging to the triclinic WO_3 phase, and the weak ones belonging to the cubic Ag phase.

The elemental compositions and chemical states of the 0.5%Ag@plate-WO_3 nanocomposite were further determined using XPS spectra. A survey scanning spectrum in Fig. 3(a) indicates that the sample consists of W, O, Ag and C. The elements of W, O and Ag belong to the 0.5%Ag@plate-WO_3 sample, and the elemental C may due to the residual PVP molecules absorbed and the carbon tape used to attach the sample powders during the XPS measurement. The W 4f spectrum shown in Fig. 3(b) has two obvious peaks at 35.1 and 37.2 eV, belonging to W $4f_{7/2}$ and W $4f_{5/2}$ of WO_3, respectively [85]. Fig. 3(c) shows the Ag 3d spectrum, which consists of two sets of peaks: one is the strong set with two peaks at 373.6 and 367.8 eV, which corresponds to the binding energies of Ag $3d_{3/2}$ and Ag $3d_{5/2}$ of metal Ag NPs, respectively [85,86]. The XPS results of Ag 3d confirm the existence of metal Ag species, agreeing with the TEM, SEM observations and XRD results (Figs. 1 and 2). Fig. 3(d) shows the high-resolution scan of C 1s, of which the weak peak with a binding energy of 286.6 eV belongs to PVP molecules adsorbed, and the strong peak at 284.6 eV should belongs to the inorganic C from the carbon tape [85]. The O 1s in Fig. 3(e) can be well fitted by two peaks centered at 529.9 and 531.3 eV, which should belong to WO_3 and PVP molecules, respectively [85]. The XPS spectra reconfirm that the 0.5%Ag@plate-WO_3 nanocomposites consist of WO_3 and metal Ag, besides a small amount of PVP molecules adsorbed.

3.2. NO-sensing response of Ag@plate-WO_3 sensors

We firstly investigated the gas-sensing properties of the Ag@plate-WO_3 sensors with various amounts of Ag NPs exposed to NO gases with various concentrations operating at 150 °C. Fig. 4 shows the typical response results operating at 150 °C. Fig. 4(a)–(e) shows the typical response (U–t) plots recorded under the NO gases with concentrations of 0.5, 1, 2, 5 and 10 ppm, respectively. One can find that the Ag@plate-WO_3 sensors are highly sensitive to a low-concentration NO gas (e.g., 0.5 ppm), and the response voltages (U) increase with the increase in the NO concentration under the testing conditions. For the NO gas with a given concentration, the Ag@plate-WO_3 sensors with various amounts of Ag NPs show different response voltages (U), and 0.5%Ag@plate-WO_3 sensor shows the largest change in response voltages (U) under gas-on and gas-off conditions, indicating that the amount of Ag NPs have a key influence on the NO-sensing property of the Ag@plate-WO_3 sensors.

Fig. 4(f) shows the change of sensitivity (R_g/R_a) as a function of the NO concentration ([NO]/ppm). The sensitivities of the Ag@plate-WO_3 sensors increase linearly with the increase in [NO] for all cases under the [NO] range of 0.5–10 ppm. For a given [NO] value, the sensitivities of the Ag@plate-WO_3 sensors operating at 150 °C have a decreasing order shown as followings: 0.5%Ag@plate-WO_3 > 0.25%Ag@plate-WO_3 > plate-WO_3 > 1%Ag@plate-WO_3 > 2%Ag@plate-WO_3. Fig. 4(g) compares the sensitivities of the Ag@plate-WO_3 sensors with various Ag amounts under different NO concentrations. One can find that the sensitivities of the Ag@plate-WO_3 sensors have maximum values at around 0.5% of Ag NPs for NO gases with various concentrations. In addition, a small amount of Ag NPs (<1%) can obviously enhance the sensitivities, whereas a large amount of Ag NPs (e.g., >2%) is unfavorable in enhancing the sensitivity of the Ag@plate-WO_3 sensors.

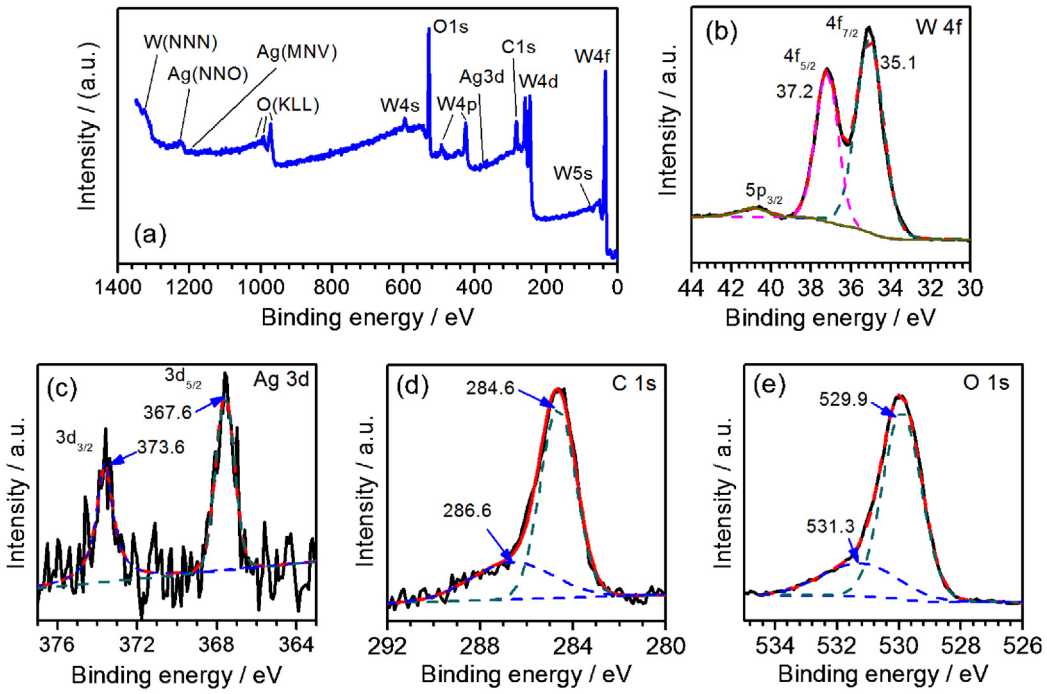

Fig. 3. XPS spectra of the 0.5%Ag@plate-WO_3 nanocomposite: (a) survey scan, (b) W 4f, (c) Ag 3d, (d) C1s, and (e) O 1s.

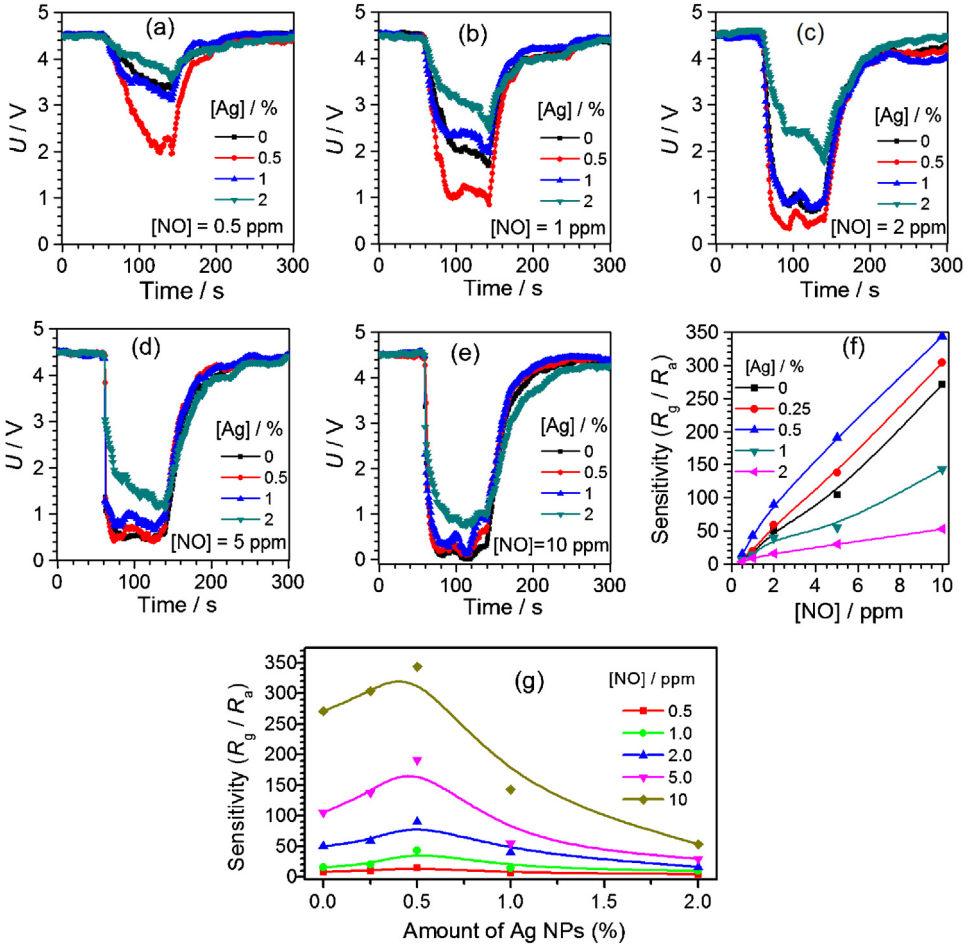

Fig. 4. (a)–(e) Typical response profiles of the Ag@plate-WO_3 sensors with various amounts of Ag NPs (0–2 wt.%) operating at 150 °C under NO gases with various concentrations: (a) 0.5 ppm, (b) 1 ppm, (c) 2 ppm, (d) 5 ppm, and (e) 10 ppm; (f) S–C curves of the Ag@plate-WO_3 sensors operating at 150 °C with R_0 = 20 MΩ; (g) change of the sensitivity as a function of the amount of Ag NPs for the Ag@WO_3-plate sensors.

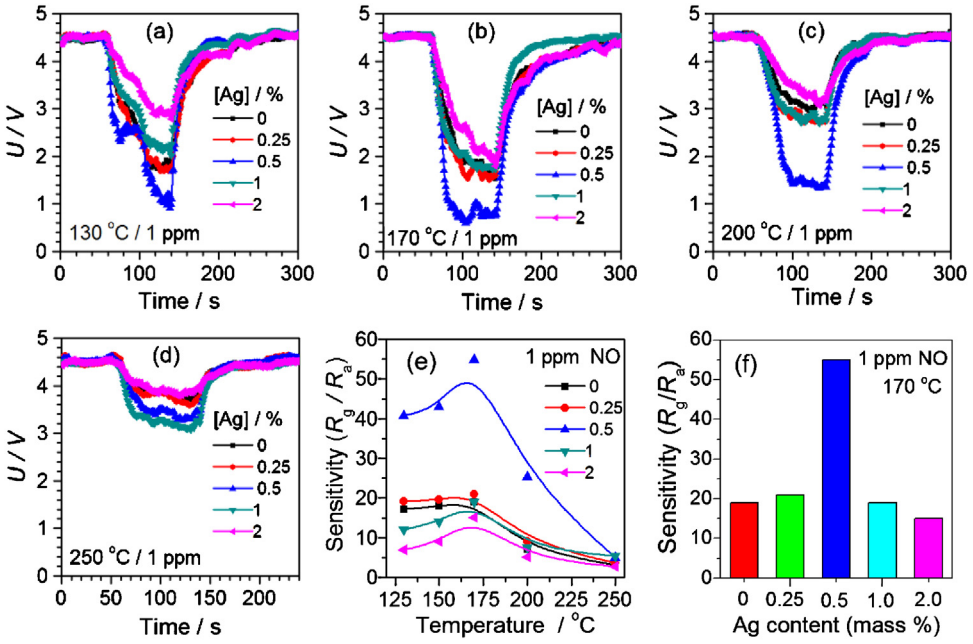

Fig. 5. (a)–(d) Response profiles of the Ag@plate-WO_3 sensors with various amounts of Ag NPs (0–2 wt.%) under 1 ppm NO gases operating various temperatures: (a) 130 °C with R_0 = 20 MΩ, (b) 170 °C with R_0 = 20 MΩ, (c) 200 °C with R_0 = 4.7 MΩ, and (d) 250 °C with R_0 = 1 MΩ; (e) S–T curves of the Ag@plate-WO_3 sensors exposed 1 ppm NO gas.

According to Fig. 4(g), the 0.5%Ag@plate-WO_3 sensor has a sensitivity of 15, 43, 90, 191 and 344 for the NO gases of 0.5 ppm, 1 ppm, 2 ppm, 5 ppm and 10 ppm, respectively, operating at 150 °C.

For SMON sensors, operation temperature is a key factor influencing their gas-sensing performance. We investigated the effects of operation temperatures on the NO-sensing performance of the Ag@plate-WO_3 sensors. Fig. 5(a)–(d) shows the typical response profiles of the Ag@plate-WO_3 sensors with various amounts of Ag NPs (0–2 wt.%) exposed to 1 ppm NO gases operating at 130–250 °C. One can see that the response changes in voltages at 150–170 °C are higher than those at 130 °C or 250 °C, indicating that the Ag@plate-WO_3 sensors have an optimum operation temperature range at 150–170 °C, and too low or too high operation temperatures are unfavorable in improving their NO-sensing performance. The plots of sensitivity versus operation temperature in Fig. 5(e) show that the Ag@plate-WO_3 sensors with various amounts of Ag NPs (0–2 wt.%) have a maximum sensitivity at around 170 °C, and the lower or higher operating temperatures lead to an obvious decrease in sensitivities for 1 ppm NO gas. The possible explanation for the above temperature-dependent response is due to the good balance of the diffusion, adsorption, reaction and desorption of the NO molecules on the Ag@plate-WO_3 sensors at 150–170 °C. The rapid and efficient diffusion and adsorption of the NO molecules are the controlling steps for the sensing response. On the one hand, high operation temperatures are helpful to accelerate the diffusion of the NO molecules and the reactions between NO molecules and the Ag@WO_3 sensors. But on the other hand, too high temperatures (e.g., 320 °C) are unfavorable to adsorption of NO on the Ag@WO_3 sensors. The temperature-dependent response phenomenon is also observed in ZnO sensors, which show the highest sensitivity at 200 °C to 200 ppm NO [30]. The sensitivity of the 0.5%Ag@plate-WO_3 sample is much higher than that of the other Ag@plate-WO_3 samples with more or less amounts of Ag NPs, as shown as Fig. 5(f).

We also investigated the low-temperature sensing performance of the Ag@plate-WO_3 sensors to a 5 ppm NO gas. Fig. 6(a) shows the room-temperature (25 °C) NO-sensing result. The Ag@plate-WO_3 sensors with various amounts of Ag NPs show perceptible response changes in voltages, and the 0.5%Ag@plate-WO_3 sensor are the most sensitive one exposed NO gases at 25 °C. When the operation temperature increases to 50 °C and 80 °C, the Ag@plate-WO_3 sensors show increasing response signals in voltage change, as shown as Fig. 6(b) and (c), respectively. Fig. 6(d) shows that the changes in sensitivity are dependent on the concentration of NO ([NO] = 0.5–50 ppm) operating at 50 °C for the Ag@plate-WO_3 sensors with various amounts of Ag NPs. One can see that the sensitivities of Ag@plate-WO_3 sensors increase with increases in the NO concentration, and the amount of Ag NPs has an important effect on the sensitivity at a low operation temperature of 50 °C: 0.5%Ag@plate-WO_3 > 1%Ag@plate-WO_3 > 0.25%Ag@plate-WO_3 > 2%Ag@plate-WO_3 > plate-WO_3. When comparing with

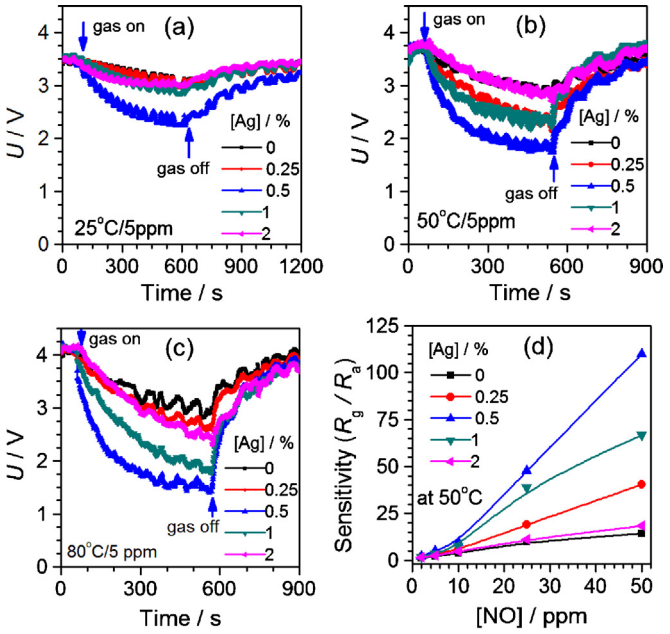

Fig. 6. (a)–(c) Low-temperature response profiles of the Ag@plate-WO_3 sensors with various amounts of Ag NPs (0–2 wt.%) under 5 ppm NO gases operating various temperatures with R_0 = 20 MΩ: (a) 25 °C, (b) 50 °C, and (c) 80 °C; (d) S–C curves of the Ag@plate-WO_3 sensors operating at 50 °C.

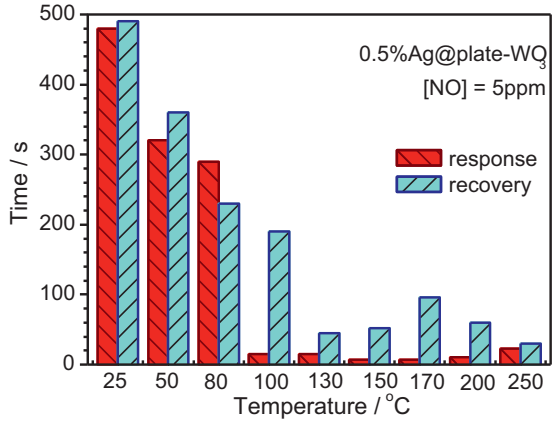

Fig. 7. Response and recovery times of the 0.5%Ag@plate-WO_3 sensor at various operation temperatures (25–250 °C) under a 5 ppm NO gas.

Figs. 4(f) and 5(e), one can find that a higher operation temperature is favorable to enhance the sensitivity of a plate-WO_3 sensor, whereas the addition of Ag NPs is favorable in low-temperature NO-sensing performance of the Ag@plate-WO_3 sensors.

Fig. 7 shows the response and recovery times of the 0.5%Ag@plate-WO_3 sensor upon exposure to a 5 ppm NO gas operating at various temperatures (25–250 °C). One can see that the enhancement in operation temperature is helpful to shorten the response and recovery times. The response and recovery times of the 0.5%Ag@plate-WO_3 sensor at 25–80 °C are about 250–500 s, and the response time can reduce to about 10 s when the operation temperature is higher than 100 °C.

3.3. *Selective gas-sensing performance of Ag@plate-WO_3 sensors to different gaseous substrates*

We comparatively investigated the selectivity of the plate-WO_3 and 0.5%Ag@plate-WO_3 sensors to various gases or vapors at an operation temperature of 200 °C. Fig. 8(a) shows the sensitivities of the plate-WO_3 and 0.5%Ag@plate-WO_3 sensors to hydrogen (100 ppm), CO (100 ppm), NO (2 ppm), acetone (100 ppm), ethanol (100 ppm), isopropanol (100 ppm), methanol (100 ppm), methanol (100 ppm) and benzene (100 ppm), respectively. One can find that the plate-WO_3 and 0.5%Ag@plate-WO_3 sensors are selectively sensitive to NO gas. In addition, the 0.5%Ag@plate-WO_3 sensor has a higher sensitivity than the plate-WO_3 sensor for the cases of NO, acetone, ethanol and isopropanol. For hydrogen, CO, methanol, methanol and benzene, both the plate-WO_3 and 0.5%Ag@plate-WO_3 sensors have low sensitivities at the testing conditions. The enhanced sensitivity and high selectivity of the Ag@plate-WO_3 sensors to NO gas is significant for practical applications. The improvement in selectivity by adding noble metals is also observed in Au-MCNT sensors for NO_2 gas [32].

Fig. 8(b) shows the selectivity of the 0.5%Ag@plate-WO_3 sensor to various gases or vapors operating at various temperatures (150–250 °C). It is interesting that the sensitivity to NO gas increases with decreases in operation temperature, whereas the sensitivity to the other gases or vapors decreases when the operation temperature decreases from 250 °C to 150 °C. In another words, the 0.5%Ag@plate-WO_3 sensor is suitable for NO detection at low operation temperature (e.g., less than 200 °C) due to its high sensitivity and selectivity to NO gases.

The sensitive and interference effect of NO with NO_2 and SO_2 on the 0.5%Ag@WO_3 sensor were also investigated. Fig. 9 shows the typical results of the 0.5%Ag@WO_3 sensor at operation temperatures of 150–300 °C to different combinations of NO, NO_2 and SO_2. One can find that the 0.5%Ag@WO_3 sensor shows a good selective response to NO and SO_2 at 150–300 °C, and has a similar response trend to NO and NO_2 at various concentrations (0.5–10 ppm). The sensitivities to SO_2 are low (less than 5) even to a high-concentration SO_2 (100 ppm) at testing temperatures of 150–300 °C, whereas the sensitivities to low-concentration NO (e.g., 0.5–10 ppm) are larger than 20 at 150–300 °C. In addition, the SO_2-sensing performance on the 0.5%Ag@WO_3 sensor shows a reverse temperature between 150 °C and 250 °C, lower than that of the literature [87]. The 0.5%Ag@WO_3 sensor shows enhanced sensitivities to the combinational gases of ($NO + NO_2$) and ($NO + SO_2 + NO_2$), when one compares them with the sensitivities of the pure NO at various operation temperatures. The sensitivities of the 0.5%Ag@WO_3 sensor to the mixed gases, i.e., ($NO + NO_2$) and ($NO + SO_2 + NO_2$), are almost the sum of their individual sensitivities under the similar testing conditions. It suggests that the 0.5%Ag@WO_3 sensor has an efficient sensing to NO_x (NO or NO_2) gases, the detection of which is not interfered by SO_2.

3.4. *Effects of the morphologies of WO_3 nanocrystals on the NO-sensing performance of Ag@WO_3 sensors*

The morphologies of the WO_3 nanocrystals, including shapes and particle-sizes, have important effects on the gas-sensing performance of the WO_3-related sensors. Fig. 10 shows the NO-sensing results of WO_3 nanoplates, 0.5%Ag@plate-WO_3, WO_3 nanoparticles, and 0.5%Ag@particle-WO_3 sensors at various operation temperatures (100–170 °C). As the figure shows, the 0.5%Ag@plate-WO_3 sensor shows the highest sensitivities among the tested samples. At 130–170 °C, the sensitivities of the sensors have a decreased order as 0.5%Ag@plate-WO_3 > WO_3

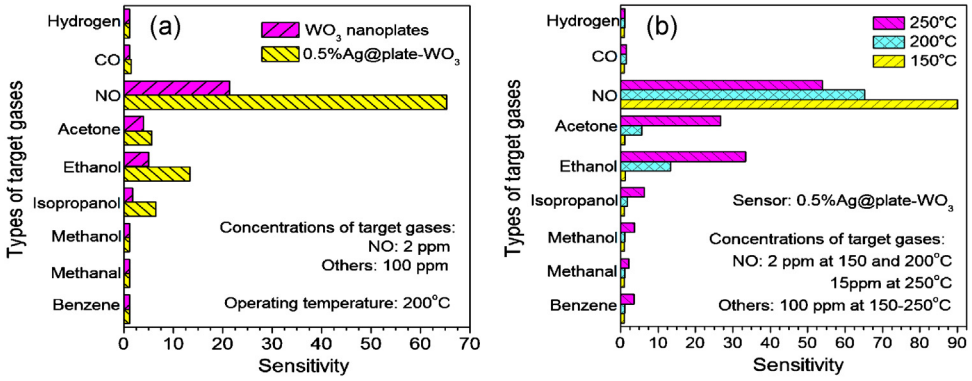

Fig. 8. (a) Comparison of the selective response of the 0.5%Ag@ plate-WO_3 sensor to different gases operating at 200 °C, and (b) selective response of the 0.5%Ag@ plate-WO_3 sensor to different target gases operating at 150–250 °C.

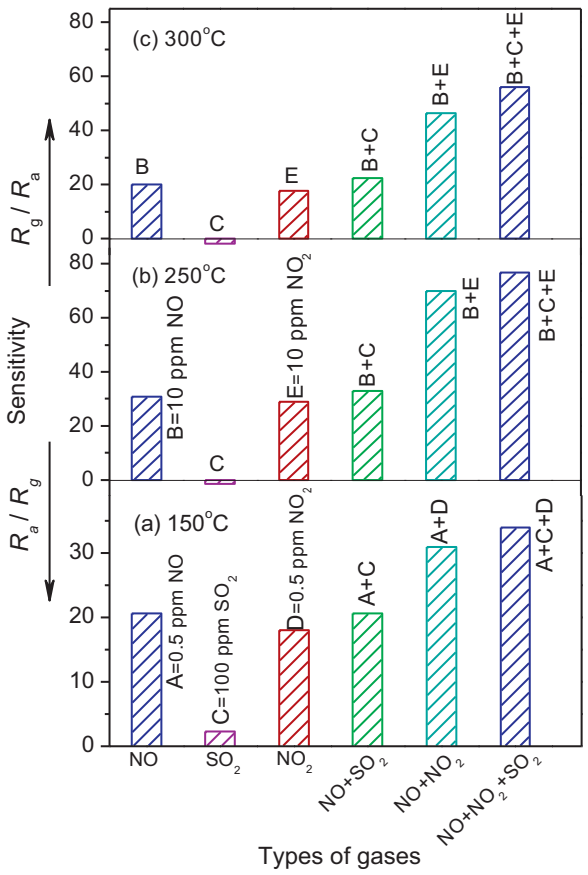

Fig. 9. Sensitivities of the 0.5%Ag@plate-WO_3 sensors to various gas combinations of NO, SO_2 and NO_2 at different operation temperatures (A = 0.5 ppm NO, B = 10 ppm NO, C = 100 ppm SO_2, D = 0.5 ppm NO_2, E = 10 ppm NO_2): (a) 150 °C, (b) 250 °C, and (c) 300 °C.

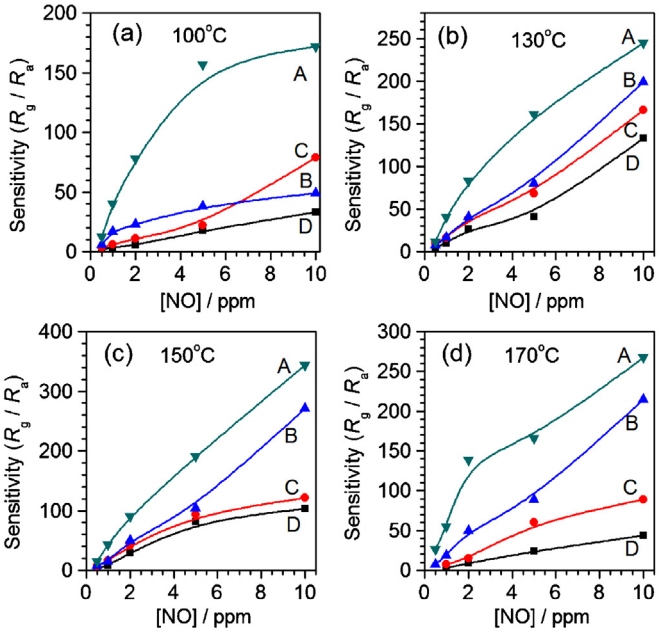

Fig. 10. Comparison of the sensitivity as a function of NO concentration for the sensors with 0.5%Ag@plate-WO_3 (A), WO_3 nanoplates (B), 0.5%Ag@particle-WO_3 (C), and WO_3 nanoparticles (D) at various operating temperatures: (a) 100 °C, (b) 130 °C, (c) 150 °C and (d) 170 °C.

nanoplates > 0.5%Ag@particle-WO_3 > WO_3 nanoparticles under a similar condition. At a low operation temperature of 100 °C, the 0.5%Ag@plate-WO_3 sensor shows a much higher sensitivity than the other WO_3-related sensors. The results indicate that the plate-like morphology of WO_3 nanocrystals is favorable in enhancing the NO-sensing performance at low operation temperatures.

3.5. Comparisons of the Ag@plate-WO_3 sensors with other NO_x-sensing sensors

Tsang et al. [69] have investigated the effects of Ag species on the NO-sensing property of the WO_3-based sensors, and found that the 1%Ag-doped WO_3 (average particle size: 300 nm) sensor showed sensitivity as high as 38.3 at an optimum operation temperature of 250 °C to 40 ppm NO in air. Penza et al. [88] investigated WO_3 thin film sensors activated by noble metals (Pd, Pt, Au) layers, and found that the thicknesses of the noble metals layers influenced the NO-sensing performance at optimum operation temperatures of 150–200 °C: the WO_3 thin film with a 30 nm Pd activation layer having the highest sensitivity of ~50–440 ppm NO and the response time ranging in several minutes. Wang et al. [89] investigated the sensing property of the WO_3-based materials with 1 wt.% metal oxides to NH_3 and NO at 350 °C, and found that the additives of Mg, Zn, Mo, and Re oxides showed good responses to 40 ppm NO, but their sensitivities at the testing conditions were lower than 10. Rao et al. [70] reported a NO-sensor based on WO_3 nanowires with diameters of 5–15 nm, and it had the highest sensitivity of ~20–10 ppm NO at an optimum operation temperature of 250 °C. Ying et al. [29] found that the 2%Al_2O_3-coated 75% SnO_2–25% $InO_{1.5}$ nanocomposite sensor shows a sensitivity of ~100–1.0 ppm NO at 150 °C due to the high adsorption to NO. In the present work, the 0.5%Ag@plate-WO_3 sensor shows an optimum operation temperature range at 150–170 °C (Fig. 5), short response times (less than 10 s, Fig. 7), and high sensitivities to NO gas (e.g., 55 for 1 ppm NO, 90 for 1 ppm NO, Fig. 4). In addition, the Ag@plate-WO_3 sensors have unique response to NO at low operation temperature 25–80 °C. When comparing the literature data with the presented results, one can readily find that the Ag@plate-WO_3 sensors reported here show an lower optimum operation temperature, more rapid response, and higher sensitivities to low-concentration NO gas. The high NO-sensing selectivity of the Ag@plate-WO_3 sensors to various gases (Figs. 8 and 9) is another advantage over these literature reported before [69,70].

3.6. Possible mechanism for the enhanced NO-sensing performance of Ag@plate-WO_3 sensors

WO_3 is an *n*-type semiconducting metal oxide. In air, O_2 molecules are adsorbed on the surfaces of the WO_3 nanoplates, and then transfer to O^-, O^{2-}or O_2^- ions by gaining electrons from the conductive band of WO_3 nanoplates at an elevated temperature, forming a electron-deleted area with a high resistance, as shown as process 1 in Fig. 11(a). When exposed to reducing gases (e.g., ethanol, acetone, CO, H_2, etc.), the WO_3 nanoplates can obtain electrons and enhance their conductivity [19,68]. When exposed to oxidizing gases (e.g., NO, NO_2, etc.), the WO_3 nanoplates lose electrons to form depletion layers and enhance their resistance.

Ag NPs enhance the NO-sensing performance of the plate-WO_3 sensors by improving the selectivity and reducing the operation temperature. The possible mechanism can be understood from the following aspects. Firstly, Ag NPs act as the active sites to enhance the selective adsoption of NO molecules, as shown as process 2–3 in Fig. 11(a). NO is a polar molecule with positive charge localized on the nitrogen and negative charge on one of the oxygen atoms, and electron interaction with the Ag NP will repel the negatively charged oxygen and attract the positively charged nitrogen

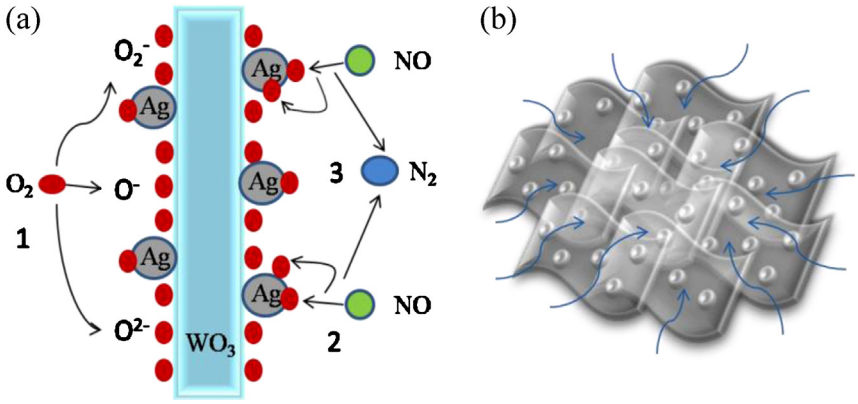

Fig. 11. (a) Schematic description of the absorption and reaction of O_2 and NO molecules on the surfaces of the Ag@plate-WO_3 nanocomposite, and (b) loose Ag@plate-WO_3 aggregates of with a house-of-card structure.

[32]. Secondly, the Schottky defects at the interface of Ag–WO_3 can reduce the activation energy and accelerate the reaction rate, resulting in enhancement of the gas-sensing performance.

Compared with Ag@particle-WO_3 sensors, the enhanced NO-sensing performance of Ag@plate-WO_3 sensors should be attributed to the loose aggregates of WO_3 nanoplates with a house-of-card structure, as shown as Fig. 11(b). This loose structure is favorable in rapid diffusion of NO molecules [68].

4. Conclusions

Novel Ag@plate-WO_3 nanocomposites were synthesized by photo-induced growth of Ag NPs on WO_3 nanoplates. Ag NPs enhanced the sensitivity of the Ag@plate-WO_3 sensors for NO detection. The amounts of Ag NPs influenced the NO-sensing performance of the Ag@plate-WO_3 sensors, and the 0.5%Ag@plate-WO_3 sample with 0.5% (in mass) Ag NPs showed the best NO-sensing property at a large operation temperature range of 25–200 °C to 0.5–100 ppm NO gases. The optimum operation temperature of the Ag@plate-WO_3 sensors was around 170 °C, but they had an obvious response at low temperatures, even at room temperature. The NO-sensing performance of the Ag@plate-WO_3 sensors was characteristic of high selectivity to various gases (i.e., H_2 and CO) or organic vapors (i.e., alcohol, acetone, methanol and benzene). The morphology of WO_3 nanocrystals also influenced the NO-sensing performance of the Ag@WO_3 sensors, and the plate-like WO_3 was prior to particle-like WO_3. The enhancement in NO-sensing performance of the Ag@plate-WO_3 sensors was attributed to the functional modification of Ag NPs and to the loose aggregates of WO_3 nanoplates with a house-of-card structure.

Acknowledgements

This work was supported by the National Natural Science Foundation of China (Grant Nos. 50802090 and 51172211), the China Postdoctoral Science Foundation(Grant Nos. 20090450094 and 201003397), the Foundation for University Young Key Teacher by Henan Province (Grant No. 2011GGJS-001), and the Advanced Programs of Returned Overseas Researchers of Henan Province (Grant No. [2011] 17). D. Chen is very grateful to Prof. Hongxia Lu, Prof. Hongliang Xu, Prof. Hailong Wang and Prof. Daoyuan Yang for their kind helps in some experiments.

References

[1] P. Grundler (Ed.), Chemical Sensor: An Introduction for Scientists and Engineers, Springer, Berlin, 2007.
[2] J. Kong, N.R. Franklin, C. Zhou, M.G. Chapline, S. Peng, K. Cho, H. Dai, Nanotube molecular wires as chemical sensors, Science 287 (2000) 622–625.
[3] H. Gu, Z. Wang, Y. Hu, Hydrogen gas sensors based on semiconductor oxide nanostructures, Sensors 12 (2012) 5517–5550.
[4] N. Barsan, D. Koziej, U. Weimar, Metal oxide-based gas sensor research: how to? Sensors and Actuators B: Chemical 121 (2007) 18–35.
[5] Z. Jing, J. Zhan, Fabrication and gas-sensing properties of porous ZnO nanoplates, Advanced Materials 20 (2008) 4547–4551.
[6] H. Yin, K. Yu, H. Peng, Z. Zhang, R. Huang, J. Travas-Sejdic, Z. Zhu, Porous V_2O_5 micro/nano-tubes: synthesis via a CVD route, single-tube-based humidity sensor and improved Li-ion storage properties, Journal of Materials Chemistry 22 (2012) 5013–5019.
[7] H. Zheng, J.Z. Ou, M.S. Strano, R.B. Kaner, A. Mitchell, K. Kalantar-zadeh, Nanostructured tungsten oxide – properties, synthesis, and applications, Advanced Functional Materials 21 (2011) 2175–2196.
[8] N. Donato, G. Neri, Plasma technologies in the synthesis and treatment of nanostructured metal oxide semiconductors for gas sensing: a short review, Nanoscience and Nanotechnology Letters 4 (2012) 211–227.
[9] J.Y. Park, S.-W. Choi, S.S. Kim, Junction-tuned SnO_2 nanowires and their sensing properties, Journal of Physical Chemistry C 115 (2011) 12774–12781.
[10] Y. Qin, F. Zhang, Y. Chen, Y. Zhou, J. Li, A. Zhu, Y. Luo, Y. Tian, J. Yang, Hierarchically porous CuO hollow spheres fabricated via a one-pot template-free method for high-performance gas sensors, Journal of Physical Chemistry C 116 (2012) 11994–12000.
[11] L. Francioso, C. De Pascali, S. Capone, P. Siciliano, Effect of top–down nanomachining on electrical conduction properties of TiO_2 nanostructure-based chemical sensors, Nanotechnology 23 (2012) 095302.
[12] N. Singh, C.Y. Yan, P.S. Lee, E. Comini, Sensing properties of different classes of gases based on the nanowire-electrode junction barrier modulation, Nanoscale 3 (2011) 1760–1765.
[13] S. Tian, F. Yang, D. Zeng, C. Xie, Solution-processed gas sensors based on ZnO nanorods array with an exposed (0 0 0 1) facet for enhanced gas-sensing properties, Journal of Physical Chemistry C 116 (2012) 10586–10591.
[14] H. Ahn, H.C. Wikle, S.-B. Kim, D. Liu, S. Lee, M. Park, D.-J. Kim, Geometric effect of ZnO nanorods on ethanol sensing properties: the relative role of a seed layer, Journal of the Electrochemical Society 159 (2012) E23–E29.
[15] A. Afzal, N. Cioffi, L. Sabbatini, L. Torsi, NO_x sensors based on semiconducting metal oxide nanostructures: progress and perspectives, Sensors and Actuators B: Chemical 171–172 (2012) 25–42.
[16] M. D'Arienzo, L. Armelao, C.M. Mari, S. Polizzi, R. Ruffo, R. Scotti, F. Morazzoni, Macroporous WO_3 thin films active in NH_3 sensing: role of the hosted Cr isolated centers and Pt nanoclusters, Journal of the American Chemical Society 133 (2011) 5296–5304.
[17] M. Ahsan, T. Tesfamichael, M. Ionescu, J. Bell, N. Motta, Low temperature CO sensitive nanostructured WO_3 thin films doped with Fe, Sensors and Actuators B: Chemical 162 (2012) 14–21.
[18] C. Lopez-Gandara, J.M. Fernandez-Sanjuan, F.M. Ramos, A. Cirera, Role of nanostructured WO_3 in ion-conducting sensors for the detection of NO_x in exhaust gases from lean combustion engines, Solid State Ionics 184 (2011) 83–87.
[19] D. Chen, X. Hou, T. Li, L. Yin, B. Fan, H. Wang, X. Li, H. Xu, H. Lu, R. Zhang, J. Sun, Effects of morphologies on acetone-sensing properties of tungsten trioxide nanocrystals, Sensors and Actuators B: Chemical 153 (2011) 373–381.
[20] Y. Zhu, X. Su, C. Yang, X. Gao, F. Xiao, J. Wang, Synthesis of TiO_2–WO_3 nanocomposites as highly sensitive benzene sensors and high efficiency adsorbents, Journal of Materials Chemistry 22 (2012) 13914–13917.
[21] A. Dedigama, M. Angelo, P. Torrione, T.-H. Kim, S. Wolter, W. Lampert, A. Atewologun, M. Edirisoorya, L. Collins, T.F. Kuech, M. Losurdo, G. Bruno, A. Brown, Hemin-functionalized InAs-based high sensitivity room temperature NO gas sensors, Journal of Physical Chemistry C 116 (2011) 826–833.
[22] G. Ko, H.Y. Kim, J. Ahn, Y.M. Park, K.Y. Lee, J. Kim, Graphene-based nitrogen dioxide gas sensors, Current Applied Physics 10 (2010) 1002–1004.

[23] H. Li, Z. Yin, Q. He, H. Li, X. Huang, G. Lu, D.W.H. Fam, A.I.Y. Tok, Q. Zhang, H. Zhang, Fabrication of single- and multilayer MoS_2 film-based field-effect transistors for sensing NO at room temperature, Small 8 (2012) 63–67.
[24] J. Wüsten, K. Potje-Kamloth, Chalcogenides for thin film NO sensors, Sensors and Actuators B: Chemical 145 (2010) 216–224.
[25] K. Yu, Z. Bo, G. Lu, S. Mao, S. Cui, Y. Zhu, X. Chen, R. Ruoff, J. Chen, Growth of carbon nanowalls at atmospheric pressure for one-step gas sensor fabrication, Nanoscale Research Letters 6 (2011) 202.
[26] S. Elouali, L.G. Bloor, R. Binions, I.P. Parkin, C.J. Carmalt, J.A. Darr, Gas sensing with nano-indium oxides (In_2O_3) prepared via continuous hydrothermal flow synthesis, Langmuir 28 (2011) 1879–1885.
[27] L. Yuan, T. Hyodo, Y. Shimizu, M. Egashira, Preparation of mesoporous and/or macroporous SnO_2-based powders and their gas-sensing properties as thick film sensors, Sensors 11 (2011) 1261–1276.
[28] C.-Y. Lin, J.-G. Chen, W.-Y. Feng, C.-W. Lin, J.-W. Huang, J.J. Tunney, K.-C. Ho, Using a TiO_2/ZnO double-layer film for improving the sensing performance of ZnO based NO gas sensor, Sensors and Actuators B: Chemical 157 (2011) 361–367.
[29] J.T. McCue, J.Y. Ying, SnO_2–In_2O_3 nanocomposites as semiconductor gas sensors for CO and NO_x detection, Chemistry of Materials 19 (2007) 1009–1015.
[30] H.N. Hieu, N.M. Vuong, H. Jung, D.M. Jang, D. Kim, H. Kim, S.-K. Hong, Optimization of a zinc oxide urchin-like structure for high-performance gas sensing, Journal of Materials Chemistry 22 (2012) 1127–1134.
[31] S. Barazzouk, R.P. Tandon, S. Hotchandani, MoO_3-based sensor for NO, NO_2 and CH_4 detection, Sensors and Actuators B: Chemical 119 (2006) 691–694.
[32] Z. Zanolli, R. Leghrib, A. Felten, J.-J. Pireaux, E. Llobet, J.-C. Charlier, Gas sensing with Au-decorated carbon nanotubes, ACS Nano 5 (2011) 4592–4599.
[33] J. Zhang, X.H. Liu, S.H. Wu, B.Q. Cao, S.H. Zheng, One-pot synthesis of Au-supported ZnO nanoplates with enhanced gas sensor performance, Sensors and Actuators B: Chemical 169 (2012) 61–66.
[34] X. Liu, J. Zhang, L. Wang, T. Yang, X. Guo, S. Wu, S. Wang, 3D hierarchically porous ZnO structures and their functionalization by Au nanoparticles for gas sensors, Journal of Materials Chemistry 21 (2011) 349–356.
[35] M.A. Lim, Y.W. Lee, S.W. Han, I. Park, Novel fabrication method of diverse one-dimensional Pt/ZnO hybrid nanostructures and its sensor application, Nanotechnology 22 (2011) 035601.
[36] E. Park, O.S. Kwon, S.J. Park, J.S. Lee, S. You, J. Jang, One-pot synthesis of silver nanoparticles decorated poly(3,4-ethylenedioxythiophene) nanotubes for chemical sensor application, Journal of Materials Chemistry 22 (2012) 1521–1526.
[37] G. Zhu, Y. Liu, H. Xu, Y. Chen, X. Shen, Z. Xu, Photochemical deposition of Ag nanocrystals on hierarchical ZnO microspheres and their enhanced gas-sensing properties, CrystEngComm 14 (2012) 719–725.
[38] K. Yu, Z. Wu, Q. Zhao, B. Li, Y. Xie, High-temperature-stable Au@SnO_2 sore/shell supported catalyst for CO oxidation, Journal of Physical Chemistry C 112 (2008) 2244–2247.
[39] V.V. Bolotov, P.M. Korusenko, S.N. Nesov, S.N. Povoroznyuk, V.E. Roslikov, E.A. Kurdyukova, Y.A. Sten'kin, R.V. Shelyagin, E.V. Knyazev, V.E. Kan, I.V. Ponomareva, Nanocomposite por-Si/SnO_x layers formation for gas microsensors, Materials Science and Engineering B: Solid State Materials for Advanced Technology 177 (2012) 1–7.
[40] D.D. Frolov, Y.N. Kotovshchikov, I.V. Morozov, A.I. Boltalin, A.A. Fedorova, A.V. Marikutsa, M.N. Rumyantseva, A.M. Gaskov, E.M. Sadovskaya, A.M. Abakumov, Oxygen exchange on nanocrystalline tin dioxide modified by palladium, Journal of Solid State Chemistry 186 (2012) 1–8.
[41] X.-J. Wang, W. Wang, Y.-L. Liu, Enhanced acetone sensing performance of Au nanoparticles functionalized flower-like ZnO, Sensors and Actuators B: Chemical 168 (2012) 39–45.
[42] N. Singh, R.K. Gupta, P.S. Lee, Gold-nanoparticle-functionalized In_2O_3 nanowires as CO gas sensors with a significant enhancement in response, ACS Applied Materials and Interfaces 3 (2011) 2246–2252.
[43] L.-L. Xing, C.-H. Ma, Z.-H. Chen, Y.-J. Chen, X.-Y. Xue, High gas sensing performance of one-step-synthesized Pd–ZnO nanoflowers due to surface reactions and modifications, Nanotechnology 22 (2011) 215501.
[44] M. Yuasa, T. Kida, K. Shimanoe, Preparation of a stable sol suspension of Pd-loaded SnO_2 nanocrystals by a photochemical deposition method for highly sensitive semiconductor gas sensors, ACS Applied Materials and Interfaces 4 (2012) 4231–4236.
[45] K. Yao, D. Caruntu, S. Wozny, R. Huang, Y.H. Ikuhara, B. Cao, C.J. O'Connor, W. Zhou, Towards one key to one lock: catalyst modified indium oxide nanoparticle thin film sensor array for selective gas detection, Journal of Materials Chemistry 22 (2012) 7308–7313.
[46] I.-S. Hwang, J.-K. Choi, H.-S. Woo, S.-J. Kim, S.-Y. Jung, T.-Y. Seong, I.-D. Kim, J.-H. Lee, Facile control of C_2H_5OH sensing characteristics by decorating discrete Ag nanoclusters on SnO_2 nanowire networks, ACS Applied Materials and Interfaces 3 (2011) 3140–3145.
[47] S. Cui, H. Pu, G. Lu, Z. Wen, E.C. Mattson, C. Hirschmugl, M. Gajdardziska-Josifovska, M. Weinert, J. Chen, Fast and selective room-temperature ammonia sensors using silver nanocrystal-functionalized carbon nanotubes, ACS Applied Materials and Interfaces 4 (2012) 4898–4904.
[48] F. Wang, C. Di Valentin, G. Pacchioni, Doping of WO_3 for photocatalytic water splitting: hints from density functional theory, Journal of Physical Chemistry C 116 (2012) 8901–8909.
[49] J.-S. Lee, I.-H. Jang, N.-G. Park, Effects of oxidation state and crystallinity of tungsten oxide interlayer on photovoltaic property in bulk hetero-junction solar cell, Journal of Physical Chemistry C 116 (2012) 13480–13487.
[50] C. Costa, C. Pinheiro, I. Henriques, C.A.T. Laia, Inkjet printing of sol–gel synthesized hydrated tungsten oxide nanoparticles for flexible electrochromic devices, ACS Applied Materials and Interfaces 4 (2012) 1330–1340.
[51] K. Hara, Z.-G. Zhao, Y. Cui, M. Miyauchi, M. Miyashita, S. Mori, Nanocrystalline electrodes based on nanoporous-walled WO_3 nanotubes for organic-dye-sensitized solar cells, Langmuir 27 (2011) 12730–12736.
[52] F. Amano, M. Tian, G. Wu, B. Ohtani, A. Chen, Facile preparation of platelike tungsten oxide thin film electrodes with high photoelectrode activity, ACS Applied Materials and Interfaces 3 (2011) 4047–4052.
[53] Z.-G. Zhao, M. Miyauchi, Nanoporous-walled tungsten oxide nanotubes as highly active visible-light-driven photocatalysts, Angewandte Chemie-International Edition 47 (2008) 7051–7055.
[54] V. Srivastava, K. Jain, Highly sensitive NH_3 sensor using Pt catalyzed silica coating over WO_3 thick films, Sensors and Actuators B: Chemical 133 (2008) 46–52.
[55] J. Yoo, D. Oh, E.D. Wachsman, Investigation of WO_3-based potentiometric sensor performance (M/YSZ/WO_3, M = Au, Pd, and TiO_2) with varying counter electrode, Solid State Ionics 179 (2008) 2090–2100.
[56] S.J. Ippolito, S. Kandasamy, K. Kalantar-zadeh, W. Wlodarski, Hydrogen sensing characteristics of WO_3 thin film conductometric sensors activated by Pt and Au catalysts, Sensors and Actuators B: Chemical 108 (2005) 154–158.
[57] X. An, J.C. Yu, Y. Wang, Y. Hu, X. Yu, G. Zhang, WO_3 nanorods/graphene nanocomposites for high-efficiency visible-light-driven photocatalysis and NO_2 gas sensing, Journal of Materials Chemistry 22 (2012) 8525–8531.
[58] J. Shi, G. Hu, Y. Sun, M. Geng, J. Wu, Y. Liu, M. Ge, J. Tao, M. Cao, N. Dai, WO_3 nanocrystals: synthesis and application in highly sensitive detection of acetone, Sensors and Actuators B: Chemical 156 (2011) 820–824.
[59] S.M. Zhu, X.Y. Liu, Z.X. Chen, C.J. Liu, C.L. Feng, J.J. Gu, Q.L. Liu, D. Zhang, Synthesis of Cu-doped WO_3 materials with photonic structures for high performance sensors, Journal of Materials Chemistry 20 (2010) 9126–9132.
[60] J. Kukkola, J. Maklin, N. Halonen, T. Kyllonen, G. Toth, M. Szabo, A. Shchukarev, J.P. Mikkola, H. Jantunen, K. Kordas, Gas sensors based on anodic tungsten oxide, Sensors and Actuators B: Chemical 153 (2011) 293–300.
[61] K.I. Shimizu, K. Kashiwagi, H. Nishiyama, S. Kakimoto, S. Sugaya, H. Yokoi, A. Satsuma, Impedancemetric gas sensor based on Pt and WO_3 co-loaded TiO_2 and ZrO_2 as total NO_x sensing materials, Sensors and Actuators B: Chemical 130 (2008) 707–712.
[62] L. Reyes, A. Hoel, S. Saukko, P. Heszler, V. Lantto, C.G. Granqvist, Gas sensor response of pure and activated WO_3 nanoparticle films made by advanced reactive gas deposition, Sensors and Actuators B: Chemical 117 (2006) 128–134.
[63] L.F. Zhu, J.C. She, J.Y. Luo, S.Z. Deng, J. Chen, N.S. Xu, Study of physical and chemical processes of H_2 sensing of Pt-coated WO_3 nanowire films, Journal of Physical Chemistry C 114 (2010) 15504–15509.
[64] S. Vallejos, T. Stoycheva, P. Umek, C. Navio, R. Snyders, C. Bittencourt, E. Llobet, C. Blackman, S. Moniz, X. Correig, Au nanoparticle-functionalised WO_3 nanoneedles and their application in high sensitivity gas sensor devices, Chemical Communications 47 (2011) 565–567.
[65] X. Liu, J. Zhang, T. Yang, X. Guo, S. Wu, S. Wang, Synthesis of Pt nanoparticles functionalized WO_3 nanorods and their gas sensing properties, Sensors and Actuators B: Chemical 156 (2011) 918–923.
[66] J. Zhang, X. Liu, M. Xu, X. Guo, S. Wu, S. Zhang, S. Wang, Pt clusters supported on WO_3 for ethanol detection, Sensors and Actuators B: Chemical 147 (2010) 185–190.
[67] D. Chen, L. Gao, A. Yasumori, K. Kuroda, Y. Sugahara, Size- and shape-controlled conversion of tungstate-based inorganic–organic hybrid belts to WO_3 nanoplates with high specific surface areas, Small 4 (2008) 1813–1822.
[68] D. Chen, X. Hou, H. Wen, Y. Wang, H. Wang, X. Li, R. Zhang, H. Lu, H. Xu, S. Guan, J. Sun, L. Gao, The enhanced alcohol-sensing response of ultrathin WO_3 nanoplates, Nanotechnology 21 (2010) 035501.
[69] L. Chen, S.C. Tsang, Ag doped WO_3-based powder sensor for the detection of NO gas in air, Sensors and Actuators B: Chemical 89 (2003) 68–75.
[70] C.S. Rout, K. Ganesh, A. Govindaraj, C.N.R. Rao, Sensors for the nitrogen oxides, NO_2, NO and N_2O, based on In_2O_3 and WO_3 nanowires, Applied Physics A: Materials Science and Processing 85 (2006) 241–246.
[71] T. Hyodo, Y. Tominaga, T. Yamaguchi, A. Kawahara, H. Katsuki, Y. Shimizu, M. Egashira, NO_x sensing properties of WO_3-based semiconductor gas sensors fabricated by slide-off transfer printing, Electrochemistry 71 (2003) 481–484.
[72] J. Tamaki, T. Hashishin, Y. Uno, D.V. Dao, S. Sugiyama, Ultrahigh-sensitive WO_3 nanosensor with interdigitated Au nano-electrode for NO_2 detection, Sensors and Actuators B: Chemical 132 (2008) 234–238.
[73] L. You, Y.F. Sun, J. Ma, Y. Guan, J.M. Sun, Y. Du, G.Y. Lu, Highly sensitive NO_2 sensor based on square-like tungsten oxide prepared with hydrothermal treatment, Sensors and Actuators B: Chemical 157 (2011) 401–407.
[74] C. Zhang, M. Debliquy, A. Boudiba, H. Liao, C. Coddet, Sensing properties of atmospheric plasma-sprayed WO_3 coating for sub-ppm NO_2 detection, Sensors and Actuators B: Chemical 144 (2010) 280–288.
[75] E.K. Heidari, E. Marzbanrad, C. Zamani, B. Raissi, Nanocasting synthesis of ultrafine WO_3 nanoparticles for gas sensing applications, Nanoscale Research Letters 5 (2010) 370–373.
[76] C.Y. Lee, S.J. Kim, I.S. Hwang, J.H. Lee, Glucose-mediated hydrothermal synthesis and gas sensing characteristics of WO_3 hollow microspheres, Sensors and Actuators B: Chemical 142 (2009) 236–242.
[77] T. Kida, A. Nishiyama, M. Yuasa, K. Shimanoe, N. Yamazoe, Highly sensitive NO_2 sensors using lamellar-structured WO_3 particles prepared by an acidification method, Sensors and Actuators B: Chemical 135 (2009) 568–574.

[78] J. Zeng, M. Hu, W. Wang, H. Chen, Y. Qin, NO_2-sensing properties of porous WO_3 gas sensor based on anodized sputtered tungsten thin film, Sensors and Actuators B: Chemical 161 (2012) 447–452.
[79] E.K. Heidari, C. Zamani, E. Marzbanrad, B. Raissi, S. Nazarpour, WO_3-based NO_2 sensors fabricated through low frequency AC electrophoretic deposition, Sensors and Actuators B: Chemical 146 (2010) 165–170.
[80] S. Ashraf, C.S. Blackman, R.G. Palgrave, S.C. Naisbitt, I.P. Parkin, Aerosol assisted chemical vapour deposition of WO_3 thin films from tungsten hexacarbonyl and their gas sensing properties, Journal of Materials Chemistry 17 (2007) 3708–3713.
[81] C. Balazsi, K. Sedlackova, E. Llobet, R. Ionescu, Novel hexagonal WO_3 nanopowder with metal decorated carbon nanotubes as NO_2 gas sensor, Sensors and Actuators B: Chemical 133 (2008) 151–155.
[82] E.H. Espinosa, R. Ionescu, E. Llobet, A. Felten, C. Bittencourt, E. Sotter, Z. Topalian, P. Heszler, C.G. Granqvist, J.J. Pireaux, X. Correig, Highly selective NO_2 gas sensors made of MWCNTs and WO_3 hybrid layers, Journal of the Electrochemical Society 154 (2007) J141–J149.
[83] J. Yoo, S. Chatterjee, E.D. Wachsman, Sensing properties and selectivities of a WO_3/YSZ/Pt potentiometric NO_x sensor, Sensors and Actuators B: Chemical 122 (2007) 644–652.
[84] D. Chen, Y. Sugahara, Tungstate-based inorganic–organic hybrid nanobelts/nanotubes with lamellar mesostructures: synthesis, characterization, and formation mechanism, Chemistry of Materials 19 (2007) 1808–1815.
[85] D. Chen, T. Li, Q. Chen, J. Gao, B. Fan, J. Li, X. Li, R. Zhang, J. Sun, L. Gao, Hierarchically plasmonic photocatalysts of Ag/AgCl nanocrystals coupled with single-crystalline WO_3 nanoplates, Nanoscale 4 (2012) 5431–5439.
[86] D. Chen, S.H. Yoo, Q. Huang, G. Ali, S.O. Cho, Sonochemical synthesis of Ag/AgCl nanocubes and their efficient visible-light-driven photocatalytic performance, Chemistry: A European Journal 18 (2012) 5192–5200.
[87] Y. Shimizu, N. Matsunaga, T. Hyodo, M. Egashira, Improvement of SO_2 sensing properties of WO_3 by noble metal loading, Sensors and Actuators B: Chemical 77 (2001) 35–40.
[88] M. Penza, C. Martucci, G. Cassano, NO_x gas sensing characteristics of WO_3 thin films activated by noble metals (Pd, Pt, Au) layers, Sensors and Actuators B: Chemical 50 (1998) 52–59.
[89] X. Wang, N. Miura, N. Yamazoe, Study of WO_3-based sensing materials for NH_3 and NO detection, Sensors and Actuators B: Chemical 66 (2000) 74–76.

Biographies

Deliang Chen has been a professor at Zhengzhou University. He received his BS and MS degrees from Central South University in 1999 and 2002, respectively. Then he moved to Shanghai Institute of Ceramics, Chinese Academy of Sciences, where he received his PhD degree in materials science and engineering in 2005. From April 2005 to March 2007, he moved to Waseda University to do postdoctoral research as visiting research associate. From April 2007 to December 2012, he worked at Zhengzhou University as an associate professor. From March 2011 to March 2012, he move to KAIST as a visiting scholar supported by China government. His current research interests are focused on the fields of chemical sensors, photocatalysts, chemical synthesis of low-dimensional materials, intercalation chemistry, microwave chemistry and sonochemistry.

Li Yin studied materials science and engineering and received her BS degree from Zhengzhou University in 2002. She is currently a PhD candidate at Zhengzhou University. Her research includes the synthesis, characterization and sensing applications of metal oxides/metals complex nanocrystals.

Lianfang Ge studied materials science and engineering and received her BS degree from Zhengzhou University in 2012. She is currently a master course student at Zhengzhou University. Her research includes the synthesis, characterization and sensing applications of low-dimensional metal oxide nanocrystals.

Bingbing Fan is now a lecturer at Zhengzhou University. She received her BS and PhD degrees from Zhengzhou University in 2006 and 2010, respectively. Her research interests are focused on the fields of computational materials and superhard materials.

Rui Zhang has been a professor at Zhengzhou University and Zhengzhou Institute of Aeronautical Industry Management. He received his BS and MS degrees from Tsinghua University in 1990 and 1995, and received his PhD degree from Shanghai Institute of Ceramics, Chinese Academy of Sciences in 2004. His current research interests include metal-ceramics, electronic ceramics and ceramic matrix composites.

Jing Sun has been a professor at Shanghai Institute of Ceramics, CAS since 2006. She received her MS degree from Changchun Institute of Applied Chemistry, CAS in 1994, and received her PhD degree from Shanghai Institute of Ceramics, CAS in 1997. Her current research interests are focused on carbon nanotube composites and low-dimensional functional nanomaterials.

Guosheng Shao is Director for the Institute of Renewable Energy and Environmental Technologies and Leader for Engineering, Sports and Sciences at the University of Bolton. He earned his PhD in materials science at the University of Surrey in 1995 and thereupon worked as a research fellow and senior research fellow, until transferring to the Brunel University as Reader in Materials in 2005. He joined the University of Bolton as Professor of Materials Modelling and Simulation in 2007. His current interest covers designed materials for renewable energy and environmental applications.